JOURNAL OF AIRCRAFT
Vol. 38, No. 5, September–October 2001

Three-Dimensional Navier–Stokes Simulations for Transport Aircraft High-Lift Configurations

R. Rudnik,* S. Melber,* A. Ronzheimer,* and O. Brodersen*
DLR, German Aerospace Research Center, 38108 Brunswick, Germany

Computations of lift and drag polars for a transport aircraft wing/fuselage high-lift configuration using the MEGAFLOW code system are carried out and compared to wind-tunnel experiments. The main emphasis is laid on a comparison of the block-structured and the unstructured code modules for such type of application. For the block-structured FLOWer code in combination with a k–ω turbulence model, the numerical results are in good agreement with the available experimental data in the linear C_L range. Beyond 15-deg incidence, a strong separation near the flap cut-out is simulated, leading to an underprediction of total lift near $C_{L,\max}$ compared to the experimental data. In contrast to this, the results of the unstructured TAU code utilizing the Spalart–Allmaras turbulence model are characterized by a nearly constant lift overestimation up to maximum lift without the aforementioned separation tendency at moderate incidences. The lift overprediction in the unstructured results is attributed to the main wing and the slat upperside suction peaks, which are higher resolved by the unstructured grid. Neither code reproduces the lift breakdown beyond $C_{L,\max}$ according to the experiments. The use of preconditioning in conjunction with the FLOWer code shows only minor improvement of the accuracy, but considerable deterioration of the convergence properties, requiring improvements for routine use. Further studies will focus on the influence of geometry simplifications at the wing root in the theoretical models and its impact on the experimental evidence.

Nomenclature

C_D	=	total drag coefficient
C_L	=	total lift coefficient
c_l	=	local chord length
c_p	=	pressure coefficient
$k^{(4)}$	=	constant of fourth-order dissipation operator
M	=	Mach number
Re	=	Reynolds number
s	=	half-span
y^+	=	normal distance from a solid wall normalized with log law variables
α	=	angle of attack
δ	=	deflection angle
Λ	=	wing aspect ratio
λ	=	wing taper
Φ_{LE}	=	wing leading-edge sweep angle

Subscripts

c	=	chord
Dp	=	pressure drag
Df	=	friction drag
f	=	flap
s	=	slat
tot	=	total

Introduction

ASIDE from continuous development and increasing experience in applying flow solvers for the solution of the Reynolds averaged Navier–Stokes (RANS) equations to two-dimensional high-lift problems during the last decade, (for example, see Refs. 1–3) only few examples of three-dimensional applications for realistic aircraft configurations have been published in the recent past.[4–6] The reason is basically the high degree of geometrical complexity of deployed high-lift systems in conjunction with a variety of relevant flow features,[7] such as strong pressure gradients, pressure, or geometry-induced separation, confluence, compressibility, for which the three dimensionality leads to a drastic increase in the required simulation performance even in the linear range of the C_L–α curve. With respect to maximum lift, the reliable prediction, or rather the prediction with a known accuracy, is becoming more and more a routine task for two-dimensional multielement flows, although the influence of three dimensionality, unsteady effects, transition determination, and numerical features of the solution algorithm still requires further investigations.[3]

Nevertheless, the numerical simulation of the flow around a complete aircraft in high-lift configuration up to maximum lift conditions is one of the major areas where Navier–Stokes methods can prove their superior potential compared to widespread and comparatively efficient coupled viscous/inviscid interaction methods. The investigations in Refs. 4 and 6 show that, depending on the numerical method and available hardware, a considerable numerical effort is necessary to compute a lift and drag polar for a three-dimensional aircraft configuration. Consequently, the prime usage for RANS simulations in the near future is likely to support the understanding of detailed flow phenomena, rather than usage inside an inverse design or optimization procedure.

Thus, the main emphasis of the present paper is twofold. First, a detailed flow analysis of the DLR, German Aerospace Research Center, ALVAST wing/fuselage transport aircraft configuration[8] with deployed high-lift system is carried out. The lift and drag polars are computed, and the stall mechanisms are discussed. When the capabilities of computational fluid dynamics (CFD) methods are used, a lift and drag decomposition for the single components of the configuration is conducted, revealing the variation of the aerodynamic forces on the elements with incidence.

The second aspect of the paper is devoted to the investigation of the numerical approach. In contrast to previous studies that concentrate on a single-solution approach, such as the chimera technique in Ref. 4 or the hybrid unstructured approach of Ref. 6, the MEGAFLOW software offers the possibility to compare the capabilities of the pure block-structured and an hybrid unstructured approach. The CFD system has been developed within the national German aerospace program MEGAFLOW[9] under the leadership of DLR, German Aerospace Research Center, with the objective of efficient and accurate computations of complex industrial aircraft

Received 31 July 2000; presented as Paper 2000-4326 at the 18th Applied Aerodynamics Conference, Denver, CO, 14–17 August 2000; revision received 11 April 2001; accepted for publication 29 April 2001.

*Research Scientist, Institute of Aerodynamics and Flow Technology.

configurations based on the RANS equations. The investigation of the ALVAST high-lift configuration based on the block-structured FLOWer code has been one of two main milestones of the first project phase. Although the complexity of the configuration has been further increased compared to Ref. 5 with the present investigation by incorporating the slat and flap gaps, a general outcome of the project is that for the pure block-structured approach, the degree of complexity is limited to wing/fuselage configurations. As an alternative, the hybrid unstructured flow solver TAU has been incorporated in the MEGAFLOW project. The basic algorithmic features of the block-structured FLOWer code and the hybrid unstructured TAU code are similar. Therefore, a comparison of both methods for the computation of the ALVAST high-lift configuration with regard to efficiency, accuracy, and turn-around time is carried out. Finally, the capabilities of preconditioning for three-dimensional configurations are assessed with respect to accuracy and efficiency improvement.

Aircraft Configuration

The DLR ALVAST wind-tunnel model[8] is a 1:10 scale model of a twin-jet narrow-body commercial aircraft similar to an Airbus A320. It has been used extensively for engine–airframe investigations in cruise and high-lift configuration in various European wind tunnels such as the German–Dutch wind tunnel- (DNW-) large low-speed facility (LLF) or the ONERA S1MA tunnel. The model has a half-span of 1.72 m. Geometric specifications such as aspect ratio Λ, taper λ, and sweep angle Φ are given in Fig. 1. For the present investigation, the takeoff configuration is considered, characterized by a continuous slat with a deflection angle of $\delta_s = 20.0$ deg and a single slotted flap with a deflection angle of $\delta_s = 19.5$ deg. The flap is split in the spanwise direction by a thrust gate. Inboard and outboard flap deflection are identical. The outboard flap ends at 84% half-span; the slat extends up to the blunt wing tip.

Grid Generation

Block-Structured Grid Generation

The generation of the block-structured grid is accomplished using the grid generation module of the MEGAFLOW project, which is the interactive grid generation package MEGACADS.[10] An important feature of this code is the parametric construction of multiblock grids using the script file technique. The present grid represents an extension of the grid around the simplified wing/fuselage junction used in Ref. 5. The comparatively straightforward inclusion of the slat and flap gaps at the fuselage intersection demonstrates the benefits of the concept. The geometry setup and the generation of the baseline grid took about 3 workmonths for an experienced user, whereas the extension of the script file to include the gaps was accomplished in about 1 week. The parametric construction of the computational grid and the restart capability is appropriate to incorporate moderate changes in wing shape or the high-lift setting, once the baseline grid has been generated. The computational grid for the complete configuration consists of about 9.2×10^6 grid points. The domain is decomposed into 50 blocks. The surface grid at the wing/fuselage junction is shown in Fig. 2. An H topology is used in the spanwise direction with 128 cells on the wing. For the wing sections, embedded C-type topology grids are wrapped around the single elements with 128 cells on the slat, 378 cells on the main wing, and 168 cells on the flap surface, respectively. The wing boundary layer is resolved with 25 cells in the normal direction. The first wall spacing amounts to 10^{-5} local chordlengths, corresponding to an average y^+ of 1. There are 16 cells placed on the blunt trailing edges of the wing elements.

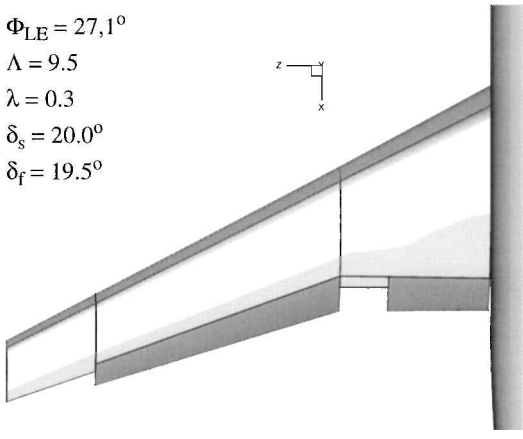

Fig. 1 Planform of DLR ALVAST model in high-lift configuration.

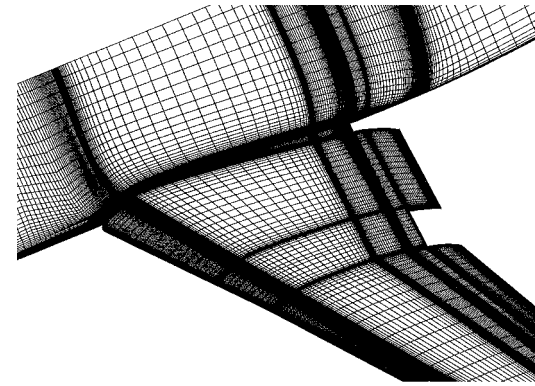

Fig. 2 Block-structured surface grid.

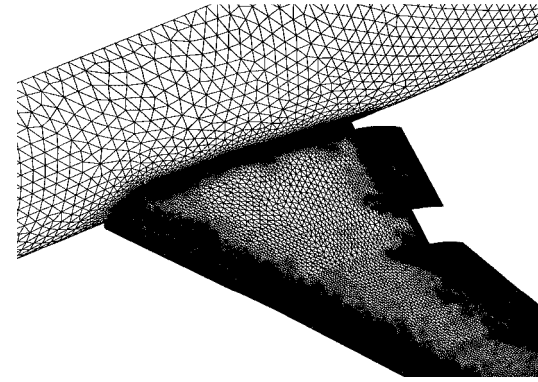

Fig. 3 Hybrid unstructured grid.

Hybrid Unstructured Grid Generation

The unstructured hybrid grid is generated with the commercial software CENTAUR,[11] using a mix of prismatic elements in the boundary-layer regions and tetrahedrons in the outer domains. A total of 4.1×10^6 grid points is used for the initial grid. The adapted grid consists of 5.8×10^6 grid points (Fig. 3). The adaptation is based on a velocity gradient sensor, resulting in a higher grid resolution at the leading edges as in the nonadapted structured grid. The first grid spacing ensures that the maximum value is limited to $y^+ = 1$ on all components. Thus, an average y^+ below 0.5 is obtained. Based on a well-defined CAD description of the model, the grid generation process requires about 1 week, depending on the grid point number, adaptation steps, and hardware availability.

Flow Solution Method

Block-Structured Flow Solver FLOWer

The FLOWer code is characterized by a cell vertex finite volume formulation of the governing equations for compressible three-dimensional flows. The baseline features of the code, as used for the present computations, are a central differencing spatial discretization of the convective fluxes with Jameson-type scalar artificial dissipation operators based on second and fourth differences of the

flow variables. Time integration to steady state is accomplished using an explicit five-stage Runge–Kutta time-stepping scheme. The convergence process is accelerated by local time stepping, implicit residual smoothing, and full multigrid technique.

For the turbulence closure, the k–ω model of Wilcox[12] is used in a slightly modified form.[13] The convective fluxes of the turbulence equations are discretized using a first-order upwind scheme. Time integration is based on a point-implicit treatment of the turbulence source terms.

Preconditioning for low Mach-number flows is implemented in the code and has been successfully applied to multielement airfoil flows in Ref. 3. Details of the numerical algorithms implemented in FLOWer are described in Ref. 14.

Hybrid Unstructured Flow Solver TAU

In contrast to the FLOWer code, the DLR TAU code is characterized by an unstructured data concept. Because the data structure is based on the edges of the control volumes, the code is independent of the type of grids cells, allowing it to handle either unstructured, structured, or hybrid grids. The governing equations are solved on a dual background grid, which is determined directly from the initial grid. As in the FLOWer code, the flow variables are stored at the cell vertices. For the discretization of the convective fluxes, several upwind or central discretization methods are available. The present computations are carried out using the second-order accurate central differencing scheme with scalar dissipation. Time integration is accomplished using an explicit three-stage Runge–Kutta scheme in conjunction with local time stepping and an agglomeration multigrid procedure. Because the implementation and validation of the k–ω turbulence model in the unstructured code is not completed, the Spalart–Allmaras model[15] is used for the present computations. For the block-structured computations, the convective fluxes of the turbulence equations are discretized using a first-order upwind scheme. No implicit source term treatment is implemented. A comprehensive description of the TAU code is given in Ref. 16.

Numerical Results

Lift and Drag Polar

The main emphasis of the investigation is the numerical simulation of the lift and drag polar using the block-structured flow solver FLOWer in continuation of the studies in Ref. 5. The experiments in Ref. 5 are conducted in the large low-speed facility of the DNW at a freestream Mach number of $M_\infty = 0.22$ and a chord Reynolds number of $Re_c = 2 \times 10^6$ (Ref. 17). Three representative angles of attack, 4, 12, and 21 deg, have been selected to demonstrate the change in flow character with increasing angle of attack. Figure 4 shows the corresponding computed isobars and wall streamlines on the wing upper surface and Fig. 5 those off the surfaces, respectively. As expected for the highest angle of attack, which corresponds to the maximum lift condition, a large-scale separation is visible. Downstream of about 30% local chord lengths, the separated flow covers nearly the complete inboard portion of the wing, extending up to the outboard flap. The wall streamlines indicate strong crossflow components, whereas the free streamlines inside the separation zones exhibit a certain streamwise alignment. This might be attributed to the higher magnitude of the velocity in the surrounding flow compared to the flow close to the wall. As Fig. 4 demonstrates, the area of the flap cutout bears the strongest separation tendency due to the missing flap effect. This is underlined by the numerical result at 4-deg incidence, which also shows a confined separation near the cutout and inboard flap, despite the low incidence. Because it is close to the design condition, the result at 12-deg incidence exhibits attached flow.

To allow a more quantitative assessment, computed pressure distributions on the slat Fig. 6, and the main wing (Fig. 7) are compared to the experimental data. The type of the slat pressure distribution changes significantly with angle of attack, the suction peak in the outboard section rises from $c_p \sim -1$ up to a value of about $c_p \sim -13$ for the highest incidence. In general, a good agreement of the FLOWer results and the experimental data is achieved.

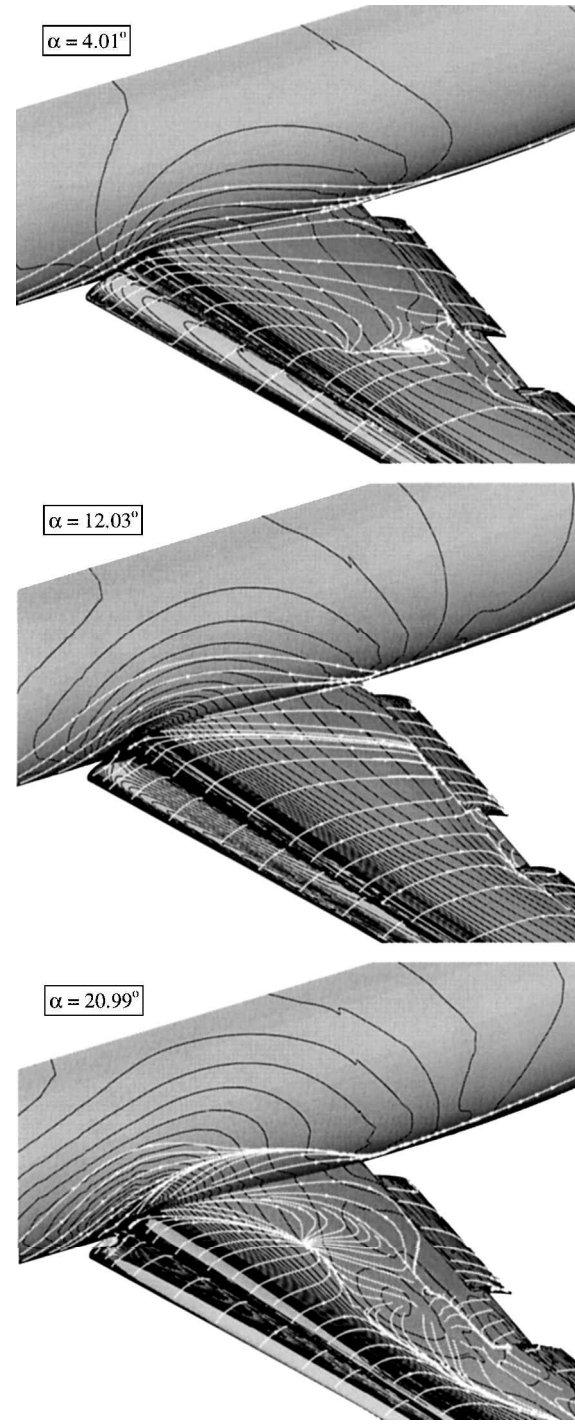

Fig. 4 Isobars and wall streamlines on wing surface.

The changes in the main wing pressure distributions are less pronounced. Again a good prediction is made for 4- and 12-deg incidence, whereas the predicted pressure distribution for the 21-deg case is characterized by an underestimation of leading-edge suction level and an overprediction of the separation at the trailing edge.

The evaluation of the corresponding lift and drag polars in Fig. 8 shows that the overestimation of the separation starts at an angle of attack of 15-deg, leading to a maximum deviation of about 5% between the measured and computed lift coefficients and about 7% for the total drag coefficient, respectively, from this incidence up to maximum lift. For lower angles of attack, the deviation between numerical and experimental simulation is about 2% for the lift and about 3% for the drag coefficients. At 22-deg angle of attack, an improved agreement between theory and experiment is observed.

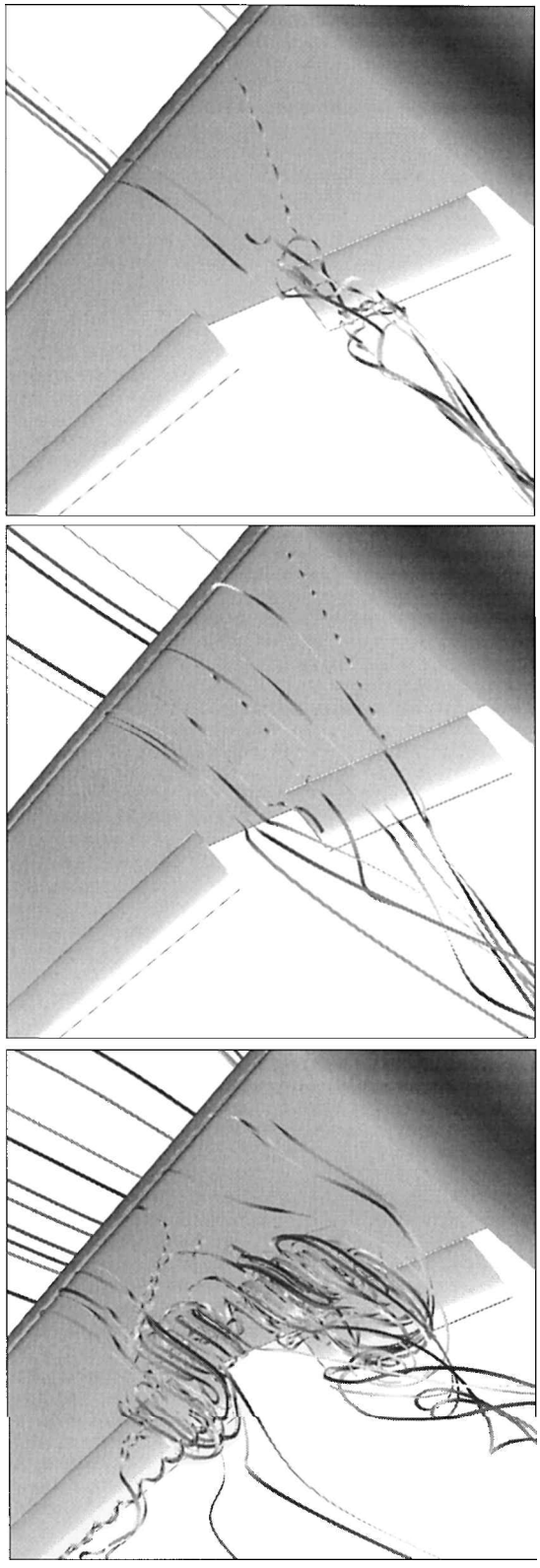

Fig. 5 Streamlines off the surface.

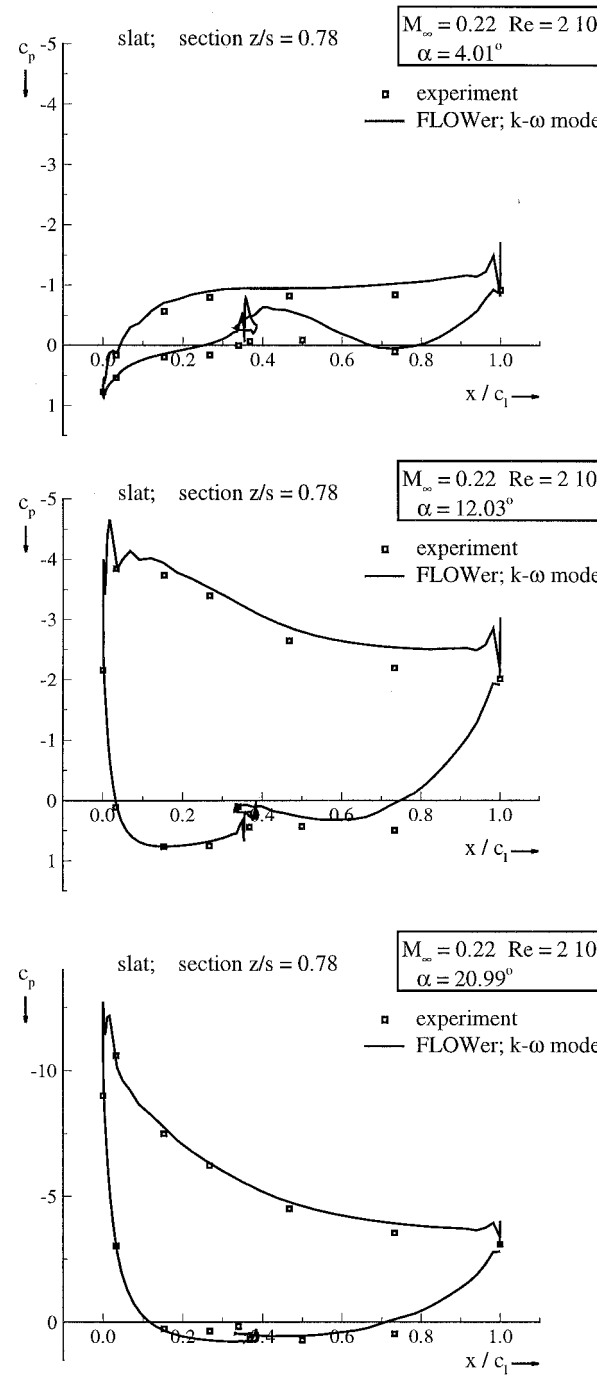

Fig. 6 Slat at 78% half-span, c_p distributions.

The analysis of this effect is carried out using the drag and lift decomposition on components as shown in Fig. 9. Comparison of the corresponding lift shares at 21 and 22 deg shows that the final increase in computed lift for the latter incidence is caused mainly by the slat and also to a certain extent by the fuselage. With respect to the experimental pressure distributions, an overprediction of the upperside pressure level on the outboard portion of the slat and wing overcompensates the midspan separation losses for 22 deg, leading to the improved agreement with the experimental lift. In general the wing contributes about two-thirds to the total lift. For the lower incidence, the fuselage provides more lift than the slat, due to the deformed pressure distributions of the slat (see also Fig. 6). For high angles of attack, the slat lift share nearly doubles that of the fuselage, corresponding to the largest C_L–α gradient of all components. The lift share of the flaps is about 7%, with a small dependency on incidence.

The drag decomposition of the numerical results obtained with the FLOWer code reveals another interesting feature of multielement high-lift configurations. Whereas all components contribute a positive share to the total drag, the slat is characterized by a negative drag component, corresponding to a suction force. This is caused by the strong suction peaks on the slat upper surface that have a considerable component in flight direction due to the slat deflection. The splitup of total drag in friction and pressure components in Table 1 proves that the friction drag of the complete configuration

Table 1 Drag breakdown on components for $\alpha = 12$ deg

Component	Pressure $C_{Dp}/C_{D,\text{tot}}$, %	Friction $C_{Df}/C_{D,\text{tot}}$, %
Fuselage	24.4	0.5
Main wing	97.0	3.6
Slat	−71.7	1.2
Flap, inboard	14.6	0.3
Flap, outboard	29.4	0.7
Σ	93.7	6.3

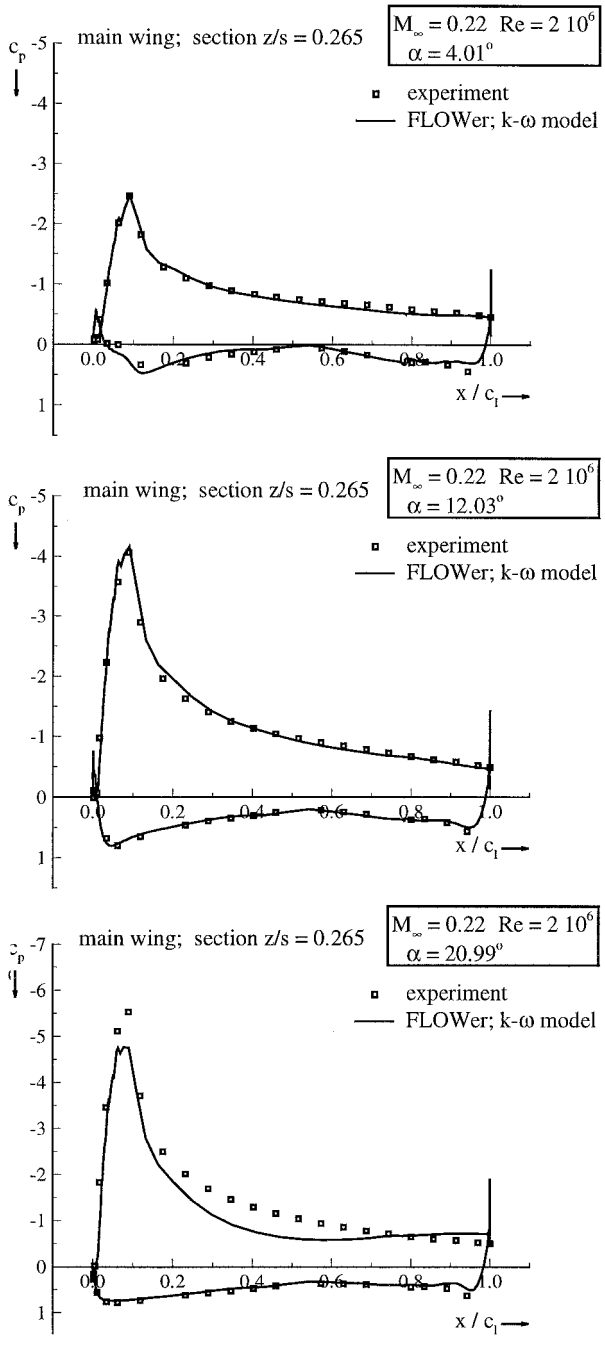

Fig. 7 Main wing at 26% half-span, c_p distributions.

contributes6.3% to the total drag. For the slat, this friction drag share decreases to about 1.5%. At the maximum lift condition, the slat suction force overcompensates the wing drag. As for the lift, the drag contribution of flap and fuselage reveals only little variations with increasing incidence. The drag evaluation indicates that a reliable drag prediction for high-lift configurations requires high accuracy with respect to the simulation of the suction peaks of the slat and also the main wing element.

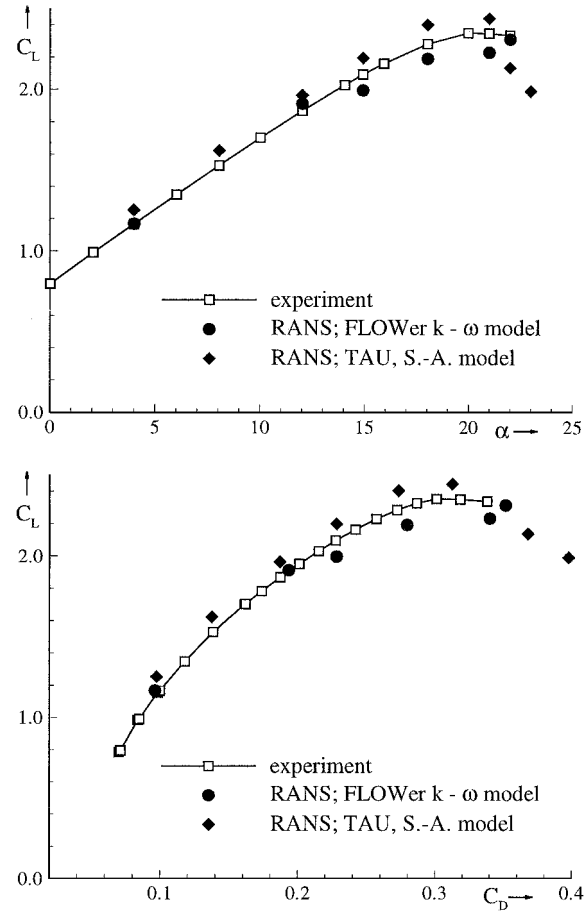

Fig. 8 Lift and drag coefficients.

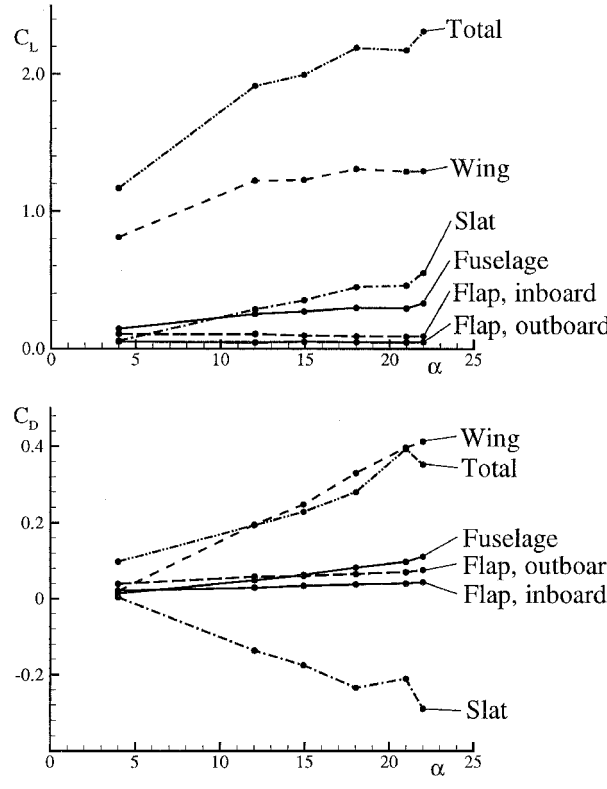

Fig. 9 Lift and drag decomposition on components.

Comparison of Block-Structured and Hybrid Unstructured Approach

The assessment of the computations carried out with the block-structured FLOWer code within the MEGAFLOW project resulted in the conclusion that the configuration complexity for this approach is limited to wing/fuselage configurations. Although no principal complexity limit exists, the effort to set up a baseline grid and the block topology in conjunction with the limited adaptation capability and low grid resolution efficiency supported the investigation of alternative approaches. The hybrid unstructured approach represents such an alternative with potential for far more complex configurations. Moreover, even if compared to the structured approach extended by chimera technique or nonmatching boundaries, the grid adaptation of the unstructured data concept offers the capability to adjust the grid resolution quite flexibly in the relevant areas of the configuration. Especially for high-lift flows, these areas change their locations considerably depending on the incidence. For these reasons, the polar computations have been repeated with the DLR TAU code utilizing the Spalart–Allmaras turbulence model.[15]

Figure 10 shows a corresponding pressure distributions at 26.5% half-span of both codes for $\alpha = 12$ deg. In general, the deviations between the results of both codes are small, most pronounced on the leading-edge suction peaks of the slat and the main wing upper surface. The reason for this deviation is attributed to the higher grid resolution at the leading edges of the respective elements in the unstructured adapted grid. The corresponding lift and drag coefficients are also marked in Fig. 8. Consistent with the higher suction peaks, the total lift coefficient is overpredicted 4.5% in the linear C_L–α range, which is about twice as much as the overprediction of the structured result. For the drag coefficient, the deviation between measurement and unstructured computation amounts to 1%, compared to 3% for the FLOWer result. Because of the higher leading-edge suction peaks in the unstructured result and the strong influence of the suction force on the pressure drag as the most important drag component, see the preceding section, the TAU result consistently produces a smaller total drag. The fact that the FLOWer result meets the drag polar for $\alpha = 12$ deg has to be attributed to a certain compensation of lift and drag overprediction. The TAU results exhibits a different stall behavior than that of the block-structured computations, meeting the slope of the experimental curve up to $C_{L,\max}$ with a nearly constant lift overprediction. At an incidence of 22 deg, the unstructured results show a comparatively sharp lift breakdown, which is not found in the experimental data. In contrast to the FLOWer results, the lift breakdown of the TAU code computation occurs primarily at the rear wing/fuselage intersection and is less pronounced at the outboard edge of the outer flap.

The convergence histories of the computations are shown in Fig. 11. The density residual has dropped more then three orders of magnitude for the block-structured code and about four orders for the unstructured code within 1000 iterations for an angle of attack of 12 deg. The changes in lift and drag coefficient are below 0.1% of the final value, which is the more relevant convergence criterion for incompressible flow solutions. The convergence of the FLOWer code levels out at two orders of magnitude in the multigrid mode. Further convergence is achieved by switching to single-grid mode after 600 iterations. The total computational time amounts to about 60 h for the block-structured computation on a NEC SX4 and about 80 h for the unstructured computation, both in a sequential mode. Near maximum lift, the number of iterations required to achieve a comparable level of convergence increases about a factor of two for the block-structured approach and about a factor of three for the unstructured approach, due to the large amount of separation, which requires more time steps until a global time-independent flowfield has established.

Influence of Spurious Dissipation

To investigate typical parameters of considerable influence on the numerical solution, the spurious dissipation, originating from the artificial dissipation terms of the main flow discretization scheme, has been varied in the block-structured computations. The dissipation term presently applied corresponds to the classical scalar dissipation model of Jameson, consisting of a blend of second- and fourth-order

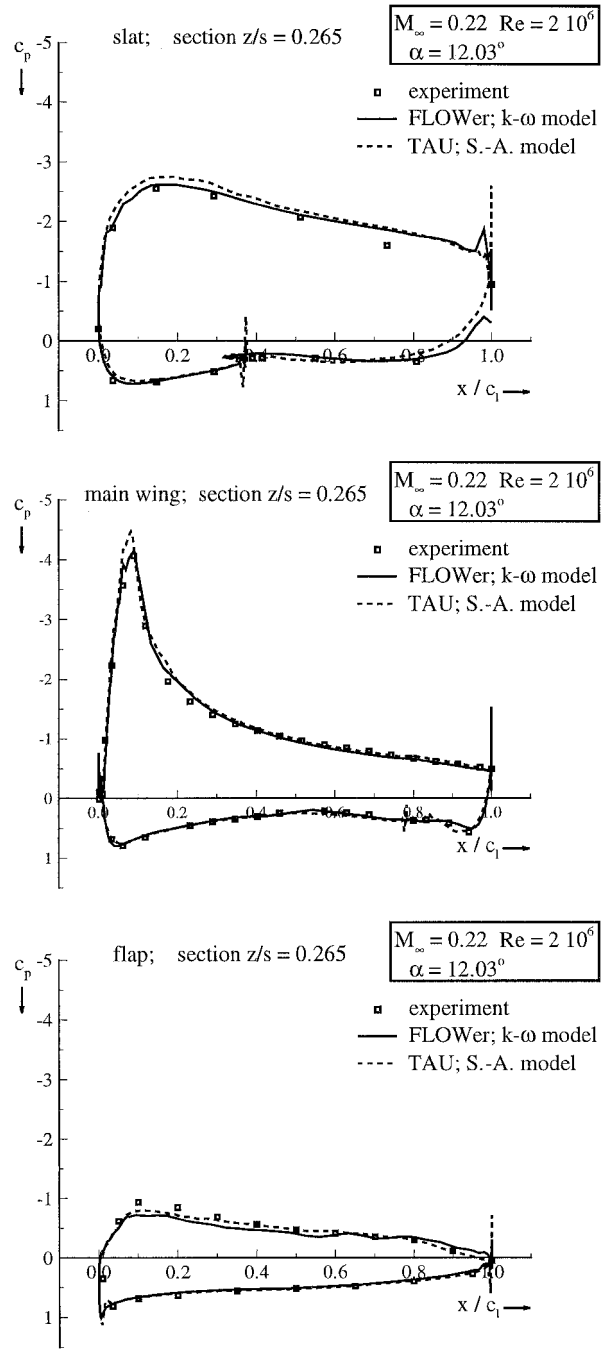

Fig. 10 Pressure coefficient c_p distributions at 78% half-span.

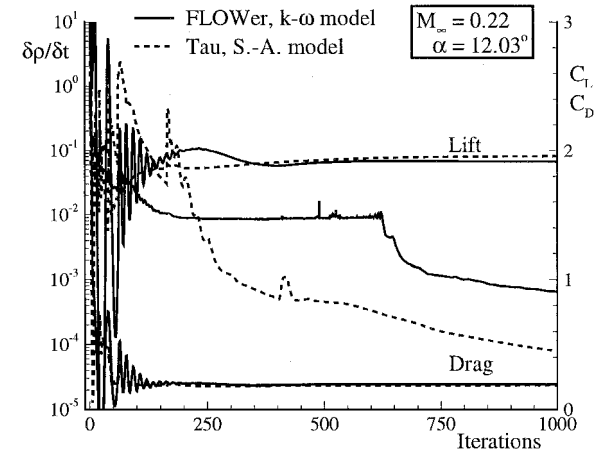

Fig. 11 Convergence history.

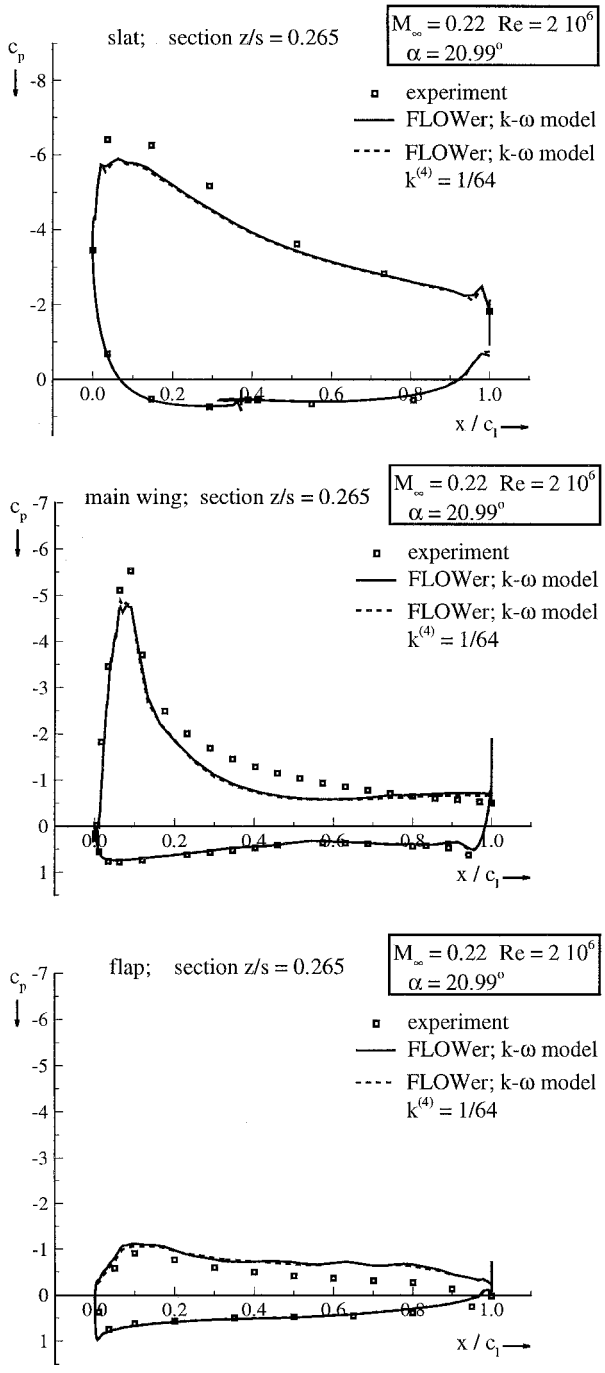

Fig. 12 Pressure coefficient c_p distributions at 26.5% half-span.

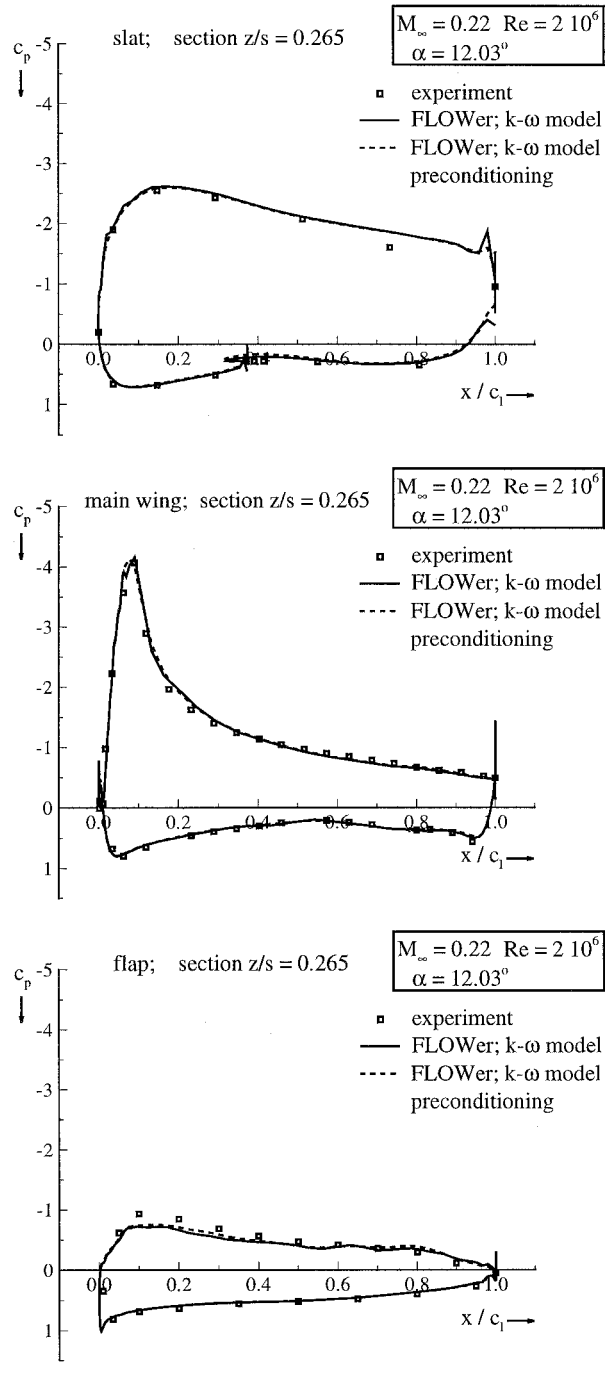

Fig. 13 Pressure coefficient c_p distributions at 26.5% half-span.

dissipation operators with the scaling factors adapted to the cell aspect ratio according to Martinelli (also see Ref. 18). For the present purpose, the constant $k^{(4)}$ in the fourth difference operator of the artificial dissipation term is halved from the baseline value $\frac{1}{32}$ to $\frac{1}{64}$. Figure 12 shows pressure distributions for the 21-deg incidence computation, which has been selected to incorporate strong gradients of the flow variables. It can be stated that the overall influence of halving the constant for the background dissipation on the pressure distribution is comparatively small. The most pronounced influence is observed on the main wing, where the leading-edge suction peak is slightly increased and the trailing edge pressure level is lowered. The impact on the overall coefficients is a decrease of 1% in lift and a 5% decrease in drag for the modified dissipation constant.

Another way to reduce the artificial dissipation is the use of preconditioning.[19] The eigenvalues of the equations for compressible flow as used in the scaling of the terms of artificial dissipation show an increasing disparity for decreasing onflow velocity that considerably influences the magnitude of the artificial dissipation. The preconditioned eigenvalues are modified to achieve a proper scaling of the dissipation terms and a higher solution accuracy and efficiency. Two-dimensional investigations of three-element airfoils[3] with preconditioning show a considerable influence on the overall coefficients, as well as a reduced robustness of the convergence properties has to be stated. For this reason, the 12-deg incidence case has been selected to assess the preconditioning influence, because it is comparatively uncritical with respect to the convergence behavior. The corresponding pressure distributions with and without preconditioning are shown in Fig. 13. The deviations between both computations are negligible; the changes in lift and drag coefficients are below 1%. Although the lift convergence is improved, the robustness of the current computations with preconditioning deteriorates by the high spikes of the mainstream residual

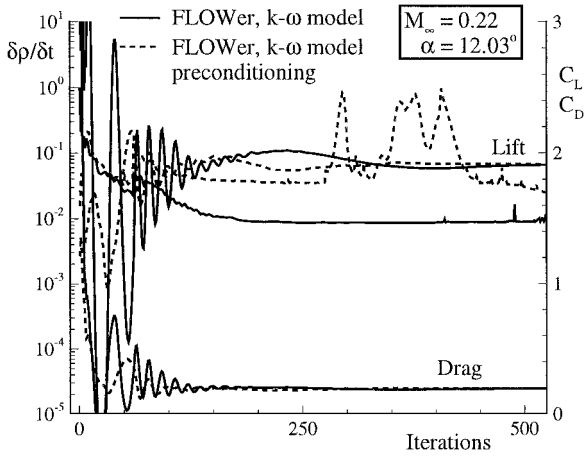

Fig. 14 Convergence history with preconditioning.

as shown in Fig. 14. This investigation shows that the implemented preconditioning technique needs further development toward improved robustness for routine use in three-dimensional high-lift applications.

Conclusions

Computations of the lift and drag polars for a wing/fuselage transport high-lift aircraft configuration are conducted with the block-structured FLOWer code and the unstructured TAU code. The comparison to experimental data reveals good agreement in pressure distributions and overall coefficients for moderate angles of attack. Beyond 15-deg incidence, the block-structured computations using a k–ω turbulence model are characterized by premature separation in the area of the flap cutout, which is not observed in the present experiments. The separation leads to a nearly constant underprediction of lift in the nonlinear range of the C_L–α curve of about 5% up to maximum lift. Beyond the experimental maximum lift incidence, this discrepancy is compensated by an underprediction of the upperside pressure level in the outboard portion of slat and main wing. The computations on the hybrid unstructured grids utilizing the TAU code and the Spalart–Allmaras turbulence model[15] on the same geometry do not exhibit this type of premature separation at moderate incidences. The angle of attack of maximum lift is fairly matched, although the maximum lift value is overpredicted about 4%. The results indicate that the stall mechanism of the experiments is not properly simulated by the theoretical approaches. Several sources of uncertainty might be responsible for the misprediction and are briefly discussed next.

1) The influence of artificial dissipation is investigated by varying the fourth differences constant and by incorporating preconditioning. Neither of the variations significantly changes the separation tendency. The overall influence on the simulation accuracy for the present grid appears to be small.

2) The turbulence model is known to have a considerable influence on separation prediction. In contrast to the block-structured k–ω model computations, the unstructured computations with the Spalart–Allmaras turbulence model[15] on the identical geometry do not produce premature separation. Nevertheless, previous studies on two-dimensional three-element airfoils[3] with the same flow solver and turbulence model show that the presently applied k–ω model tends to underpredict separation. Thus, it is unlikely that the overprediction of separation is primarily a turbulence model fault. Clarification of this aspect requires a turbulence model comparison within the same numerical code.

3) The computations have been carried out without prescribed transition because the transition location has not been detected throughout the experiment. Prescription of transition for multielement airfoils tends to increase the leading-edge suction peaks and alleviates flow separation, which holds promise to improve the observed misprediction.

4) The wind-tunnel model is equipped with an endplate at the slat edge and a fairing at the intersection between wing upperside and fuselage. Mainly because of the complexity of the block-structured grid generation, these devices have not yet been incorporated in the present computational model. In Ref. 19, a significant influence of the design of the fuselage/wing intersection on the stall mechanism is reported. This is confirmed by wind-tunnel tests of the ALVAST model in a similar high-lift setting without the slat horn and the fuselage fairing that also revealed a premature separation at moderate incidences, supporting the results of the FLOWer code in conjunction with the k–ω model. Based on the present results this item cannot be finally resolved.

The lift and drag analysis of the results reveals that the slat lift contribution shows the strongest change with increasing angle of attack, followed by wing and fuselage. The drag decomposition underlines that the pressure drag is the dominant drag component, contributing about 90% to the total drag. The drag breakdown on the single elements of the configuration shows that for high angles of attack a negative slat drag compensates the positive wing drag to a considerable degree because both are of a similar magnitude.

The computation of the configuration with the unstructured flow solver on a hybrid grid produces results of comparable accuracy to those of the block-structured approach in fair agreement with the experimental data in the linear regime of the C_L–α curve. The code efficiency in terms of lift convergence is slightly lower than that of the FLOWer code due to purely explicit time integration. Nevertheless, the convergence behavior is more robust. The simulation of the lift breakdown of both approaches is quite different. As a major outcome of the present study, the configurations with and without the lift enhancing devices at the wing/fuselage junction will have to be investigated using the hybrid unstructured TAU code with both presently used turbulence models, to assess the stall prediction capability of the numerical method. Future investigations of more complex three-dimensional configurations will be based on the unstructured approach, due to the high potential in efficient and accurate grid generation and adaptation of the grid to local flow phenomena that are of great importance especially for investigations of high lift.

References

[1]Rogers, S. E., Wiltberger, N. L., and Kwak, D., "Efficient Simulation of Incompressible Viscous Flow Over Multi-Element Airfoils," CP-515, AGARD, 1993, pp. 7-1–7-9.

[2]Larsson, T., "Separated and High-Lift Flows Over Single and Multi-Element Airfoils," International Council of the Aeronautical Sciences, ICAS Paper 94-5.7.3, 1994, pp. 2505–2518.

[3]Lindblad, I. A. A., and de Cock, K. M. J., "Computational Fluid Dynamics Prediction of Maximum Lift of a Two-Dimensional High Lift Configuration," AIAA Paper 99-3180, 1999.

[4]Cao, H. V., Su, T. Y., and Rogers, S. E., "Navier–Stokes Analyses of a 747 High-Lift Configuration," AIAA Paper 98-2623, 1998.

[5]Rudnik, R., Ronzheimer, A., and Raddatz, J., "Numerical Flow Simulation for a Wing/Fuselage Transport Configuration with Deployed High-Lift System," *Notes on Numerical Fluid Mechanics*, Vol. 72, Vieweg-Verlag, Brunswick, Germany, 1999, pp. 363–370.

[6]Mavriplis, D. J., and Pirzadeh, S., "Large-Scale Parallel Unstructured Mesh Computations for Three-Dimensional High-Lift Analysis," AIAA Paper 99-0537, 1999.

[7]Haines, A. B., and Young, A. D., "Scale Effects on Aircraft and Weapon Aerodynamics," AGARD-AG-323, 1994, pp. 27–65.

[8]Kiock, R., "The ALVAST Model of DLR," DLR, German Aerospace Research Center, DLR Institute of Design Aerodynamics, Lilienthalplatz 7, 38018 Braunschweig, Rept. IB 129-96/22, 1996.

[9]Kroll, N., Rossow, C.-C., Becker, K., and Thiele, F., "MEGAFLOW-A Numerical Flow Simulation System," International Council of the Aeronautical Sciences, ICAS-98 Paper 2.7.4, 1998.

[10]Brodersen, O., Hepperle, M., Ronzheimer, A., Rossow, C.-C., and Schöning, B., "The Parametric Grid Generation System MEGACADS," *Proceedings of the 5th International Conference on Numerical Grid Generation in Computational Field Simulations*, edited by B. K. Soni, J. F. Thompson, J. Häuser, and P. Eisemann, Mississippi State University, 1996, pp. 353–362.

[11]Kallinderis, Y., "Hybrid Grids and Their Applications," *Handbook of Grid Generation*, CRC Press, Boca Raton, FL, 1999, pp. 25-1–25-18.

[12]Wilcox, D. C., "Reassessment of the Scale Determining Equation

for Advanced Turbulence Models," *AIAA Journal*, Vol. 26, No. 11, 1988, pp. 1299–1310.

[13]Rudnik, R., "Evaluation of the Performance of Two-Equation Turbulence Models for Airfoil Flows," DLR, German Aerospace Research Center, DLR Institute of Design Aerodynamics, Lilienthalplatz 7, 38018 Braunschweig, Rept. FB 97-49, 1997.

[14]Kroll, N., "National CFD Project MEGAFLOW-Status Report," *Notes on Numerical Fluid Mechanics*, Vol. 60, Vieweg-Verlag, Brunswick, Germany, 1997, pp. 15–23.

[15]Spalart, P. R., and Allmaras, S. R., "A One-Equation Turbulence Model for Aerodynamic Flows," AIAA Paper 92-0439, 1992.

[16]Gerhold, T., Friedrich, O., Evans, J., and Galle, M., "Calculation of Complex Three-Dimensional Configurations Employing the DLR τ Code," AIAA Paper 97-0167, 1997.

[17]Puffert-Meißner, W., "ALVAST Half-Model Wind Tunnel Investigations and Comparison with Full-Span Model Results," DLR German Aerospace Research Center, DLR Institute of Design Aerodynamics, Lilienthalplatz 7, 38018 Braunschweig, Rept. IB 129-96/20, 1996.

[18]Kroll, N., Radespiel, R., and Rossow, C.-C., "Structured Grid Solvers I, Accurate and Efficient Flow Solvers for 3D Applications on Structured Meshes," AGARD R-807, 1995, pp. 4-1–4.59.

[19]Turkel, E., Radespiel, R., and Kroll, N., "Assessment of Two Preconditioning Methods for Aerodynamic Problems," *Computers and Fluids*, Vol. 26, No. 6, 1997, pp. 613–634.